

Cellular Signaling Circuits Interface with Synthetic, Post-Translational, Negating Boolean Logic Devices

Shiva Razavi,^{†,§,⊥} Steven Su,^{†,§,⊥} and Takanari Inoue^{*,§,⊥,||}

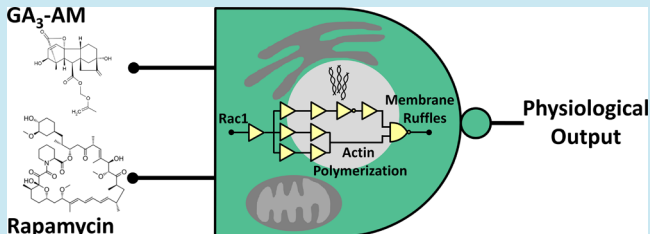
[†]Department of Biomedical Engineering, [§]Department of Cell Biology, and [⊥]Center for Cell Dynamics, Johns Hopkins University School of Medicine, Baltimore, Maryland 21205, United States

^{||}Japan Science and Technology Agency, 4-1-8 Honcho, Kawaguchi, Saitama 332-0012, Japan

Supporting Information

ABSTRACT: A negating functionality is fundamental to information processing of logic circuits within cells and computers. Aiming to adapt unutilized electronic concepts to the interrogation of signaling circuits in cells, we first took a bottom-up strategy whereby we created protein-based devices that perform negating Boolean logic operations such as NOT, NOR, NAND, and N-IMPLY. These devices function in living cells within a minute by precisely commanding the localization of an activator molecule among three subcellular spaces. We networked these synthetic gates to an endogenous signaling circuit and devised a physiological output. In search of logic functions in signal transduction, we next took a top-down approach and computationally screened 108 signaling pathways to identify commonalities and differences between these biological pathways and electronic circuits. This combination of synthetic and systems approaches will guide us in developing foundations for deconstruction of intricate cell signaling, as well as construction of biomolecular computers.

KEYWORDS: synthetic Boolean logic, negation, chemically induced dimerization, membrane ruffling, Rac, signaling pathway



Boolean logic devices that digitize and process multiple input signals are central to digital electronics. These devices function in a binary domain, are activated with higher specificity than single-input devices, and thus better tolerate environmental noise.^{1–3} Hence, devising biomolecular-based Boolean logic gates can prove promising in performing robust detection or therapeutic functions in the inherently noisy cellular environment. This class of devices also allows for interrogation of biology both on a molecular- and systems-level. While assembling biomolecular parts in a biological circuit enables reexamination of our knowledge of an individual component's function, deploying these devices in living cells facilitates real-time manipulation and assessment of cellular events.

Transcription-based Boolean logic gates have been developed and studied extensively.⁴ These devices are versatile and can be wired to each other to generate complex functions.^{5–9} However, they often take hours to days to become active as the transcription machinery dictates the speed of transcriptional-based logic operators.³ Furthermore, one class of Boolean devices (e.g., NOT, NAND, NOR, etc.) executes negation using an inhibitory module, such as a repressor that requires an added layer of regulation, leading to design complexity and increased chance of crosstalk with the endogenous molecules. Moreover, the readouts of such devices are primarily fluorescence intensity, an output that is not physiologically relevant. To achieve faster computation that is not rate-limited by transcription, logic devices utilizing the post-

translational repertoire of biomolecules have been engineered.^{3,10} For example, the primary Boolean logic functions have been developed using enzymes.^{11–13} Although these enzyme-based devices process the output on an hour-time scale,³ they are operational only *in vitro*. We previously established a system to introduce the AND and OR logic operators in living cells to generate protein-based logic devices that are functional within 1 min.¹⁴ However, implementation of more complex Boolean logic operations incorporating the NOT inverting functionality (such as NAND and NOR) remained an open challenge.

RESULTS AND DISCUSSIONS

Aiming toward the eventual construction of two-input negating logic functions in living cells, we first developed a NOT inverter (Figure 1a), an elementary component of the NOR, NAND, and N-IMPLY logic devices. For fast operation, we coded functionality in localization of a protein of interest. T-cell lymphoma invasion and metastasis-inducing protein 1 (Tiam1) is a well characterized exchange factor for Rac small GTPase¹⁵ and thus chosen as a proof of principle in this study because it could later be used as the input to downstream signaling pathways. To rapidly control localization of Tiam1, we designated three intracellular compartments as its transient hosts: the plasma membrane (PM), cytoplasm, and mitochon-

Received: March 25, 2014

Published: July 7, 2014

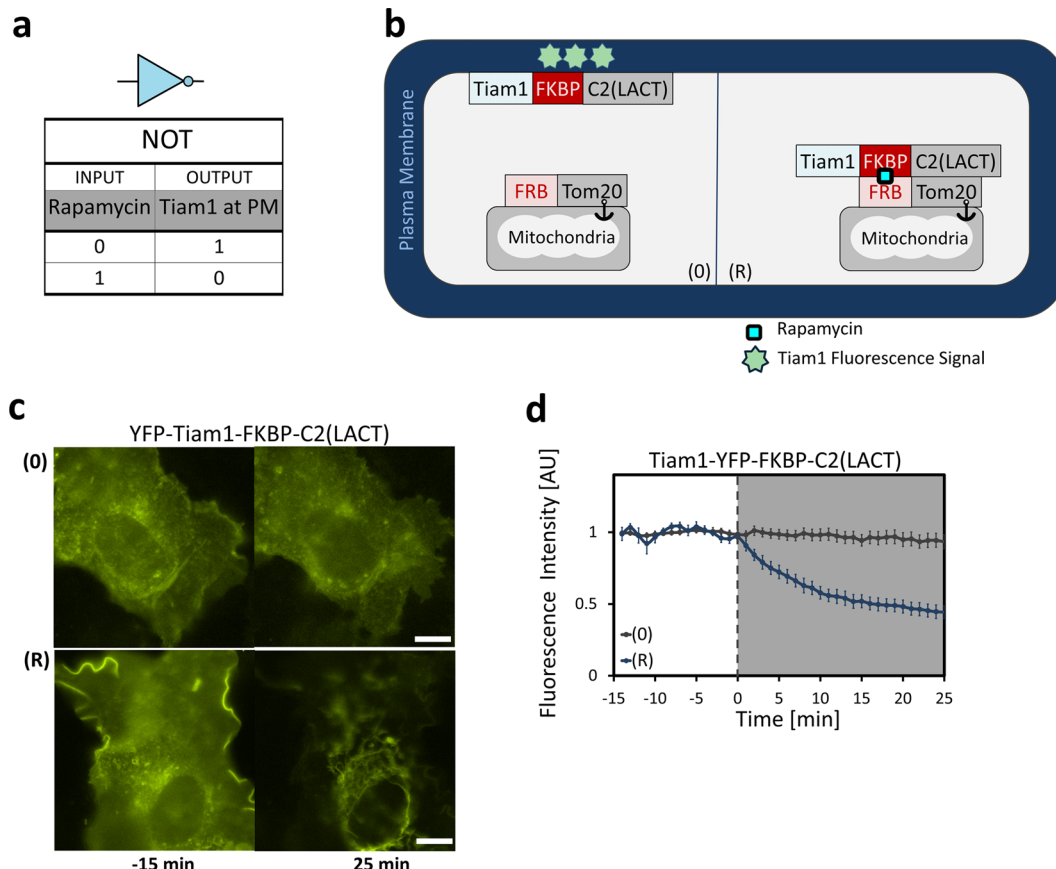


Figure 1. NOT gate. (a) NOT truth table. (b) Schematic of the protein constructs used for NOT logic implementation. For clarity, fluorescent protein components are omitted from this and subsequent diagrams. YFP-Tiam1-FKBP-C2(LACT) is at the PM and Tom20-CFP-FRB is mitochondria-bound. (0) and (R) represent the DMSO and rapamycin (100 nM) inputs, respectively. DMSO does not change the localization conditions (left panel). Rapamycin recruits YFP-Tiam1-FKBP-C2(LACT) to the mitochondria and PM ruffles disappear (right panel). (c) Representative cells showing YFP-Tiam1-FKBP-C2(LACT) localization at the initial and end time points for the (0) and (R) input conditions. The scale bars are 10 μ m. The image contrasts have been adjusted to better show relocalization. (d) Translocation dynamics of YFP-Tiam1-FKBP-C2(LACT) construct in PM upon rapamycin or DMSO addition. Fluorescence intensity is measured at the PM. Time zero intercept marks the input addition time point. The gray region highlights the time interval during which the inputs are present. Error bars depict standard error of the mean (SEM) for $n = 12$.

dria. Tiam1 presence at the PM registered a *high* output, whereas Tiam1 localization at the cytoplasm or mitochondria drove the output to a *low*. To alter the localization state of the system in a spatiotemporally controlled manner, we relocated Tiam1 between these compartments using a chemically inducible dimerization (CID) technique, whereby two protein modules dimerize upon addition of a chemical dimerizer.^{16,17} The CID system we chose consisted of FKBP (FK506 binding protein) and FRB (FKBP12 rapamycin binding protein) proteins which readily pair in the presence of rapamycin.¹⁸

For the NOT logic device, we designed two distinct fusion proteins: one with yellow fluorescent protein (YFP), actuator (Tiam1), dimerization (FKBP), and localization (C2 domain from lactadherin or C2(LACT)) protein constituents (termed YFP-Tiam1-FKBP-C2(LACT)) and the other with cyan fluorescent protein (CFP), dimerization (FRB), and localization (Tom20) elements (termed Tom20-CFP-FRB). From a design standpoint, choosing protein localization tags with appropriate affinities for their respective intracellular compartment was key in implementing negation. While the C2(LACT) transiently associates with the PM by binding to phosphatidylserine,¹⁹ Tom20 permanently anchors at the outer leaflet of the mitochondrial membrane²⁰ (Figure 1b). To monitor the

PM boundary, we expressed the two fusion proteins together with the mCherry-CAAX protein, a PM marker,²¹ in COS-7 fibroblast-like cells (Supporting Information Figure 1a). The localization of YFP-Tiam1-FKBP-C2(LACT) was biased toward the PM, leading to an initial *high* output state. This protein construct remained PM-bound upon addition of the null input of dimethyl sulfoxide (DMSO). However, adding 100 nM rapamycin triggered its translocation away from the PM toward the mitochondria where Tom20-CFP-FRB was expressed (Figure 1c). As a result the *high* fluorescence output remained unperturbed for the null input, yet for the rapamycin input, translocation occurred indicating successful implementation of the NOT device (Figure 1d). The average normalized Tiam1 fluorescence intensity at the PM was at 100% immediately before rapamycin addition and dropped to 72% 5 min post-rapamycin addition (Supporting Information Figure 1b). This change in fluorescence intensity was statistically significant ($p = 1.7 \times 10^{-3}$) at the first minute post-input addition, and thus, the NOT device was considered active at this time point (Supporting Information Figure 1c).

Using the NOT inverting device as a basis, we next set out to develop cascade-free, binary-input negating logic devices, starting with the NOR function. To retain the fast activation

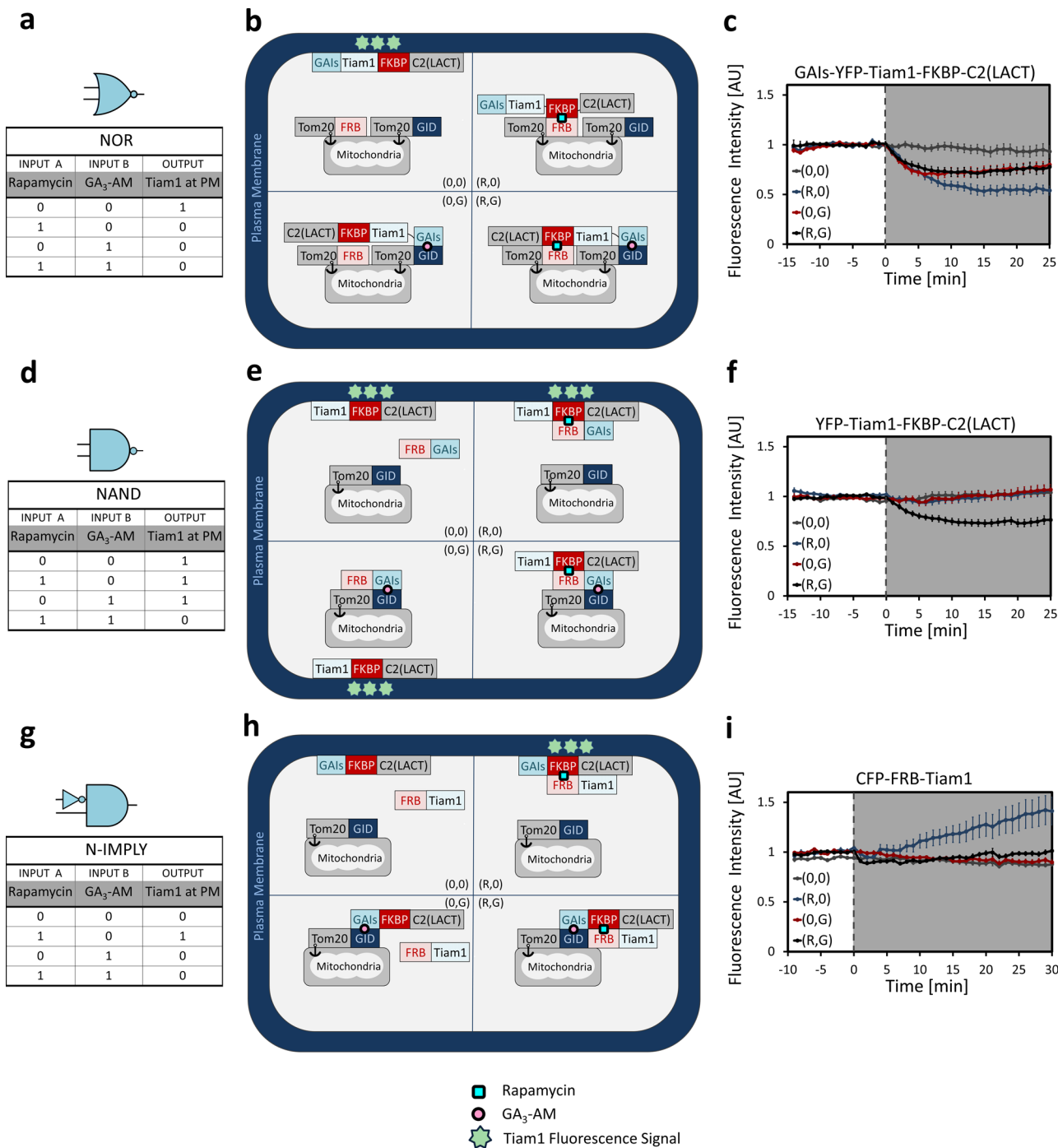


Figure 2. (a) NOR logic truth table. (b) Schematic of the localization of the NOR device protein constituents: GAIs-YFP-Tiam1-FKBP-C2(LACT) is PM-bound, Tom20-CFP-FRB, and Tom20-mCherry-GID are at mitochondria. PM fluorescence only exists for the DMSO condition (top left panel). Addition of rapamycin (100 nM), GA₃-AM (10 μ M), or both, relocates GAIs-YFP-Tiam1-FKBP-C2(LACT) toward the mitochondria. (c) Translocation dynamics of GAIs-YFP-Tiam1-FKBP-C2(LACT) at PM upon addition of various combination of inputs. (d) NAND logic truth table. (e) Schematic of the localization of the NAND device protein constituents: YFP-Tiam1-FKBP-C2(LACT) is at the PM, Tom20-mCherry-GID is anchored at the mitochondria, FRB-mCherry-GAIs is cytosolic. DMSO, Rapamycin (100 nM) and GA₃-AM (10 μ M) alone fail to sequester YFP-Tiam1-FKBP-C2(LACT) from the PM, and the PM fluorescence remains high. Rapamycin and GA₃-AM together, result in the recruitment of YFP-Tiam1-FKBP-C2(LACT)/mCherry-FRB-GAIs complex to the mitochondria, and the output is driven to a low state. (f) Translocation dynamics of YFP-Tiam1-FKBP-C2(LACT) construct at the PM upon addition of the inputs. (g) N-IMPLY logic truth table. (h) Diagram depicting the location of each protein construct. GAIs-YFP-FKBP-C2(LACT) expresses at the PM, CFP-FRB-Tiam1 is cytoplasmic, and Tom20-mCherry-GID is mitochondrial bound. Tiam1 translocation to the PM only takes place once rapamycin (100 nM) alone is present. Presence of GA₃-AM (100 μ M) obstructs permanent translocation of the Tiam1 to the PM. (i) Translocation dynamics of CFP-FRB-Tiam1 at the PM. The binary inputs are denoted as follows: (0,0) for DMSO, (R,0) for rapamycin, (0,G) for GA₃-AM, (R,G) for rapamycin and GA₃-AM, both. Time zero intercept marks the input addition time point. All error bars depict SEM for $n \geq 12$. The scale bars are 10 μ m.

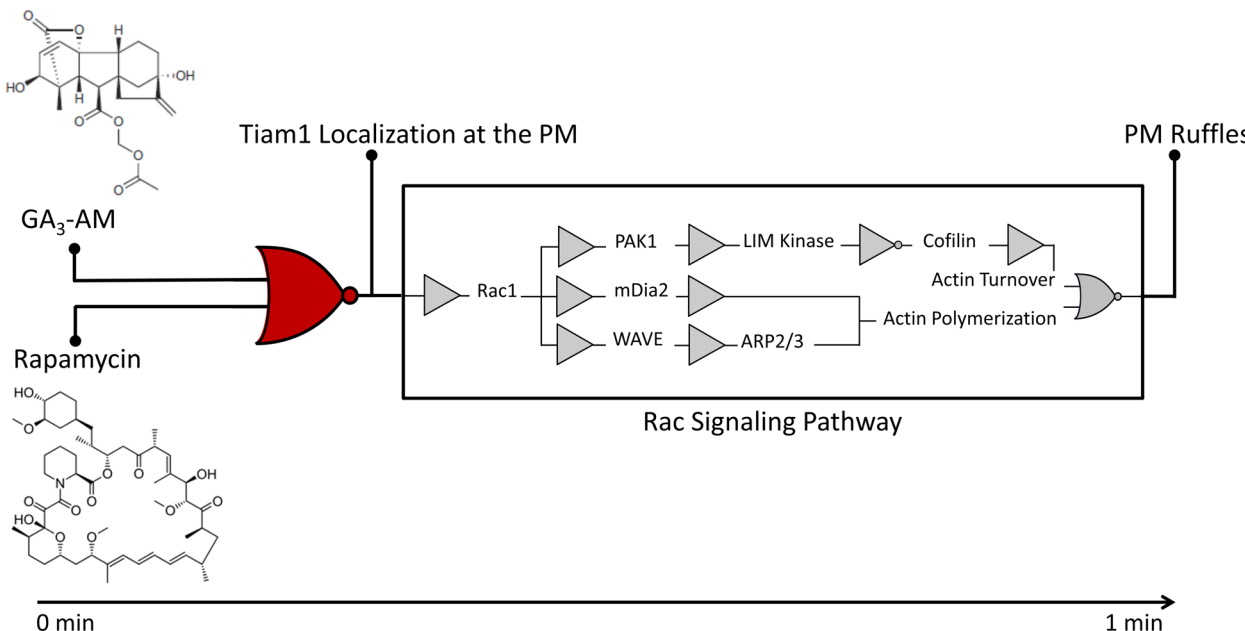


Figure 3. For the synthetic logic device, chemical dimerizers serve as the binary inputs, and the Tiam1 localization at the plasma membrane dictates the output. Cascading the device to the endogenous Rac generates the second output of plasma membrane ruffles.

time, we continued to use the CID platform. As the NOR truth table suggests (Figure 2a), this gate requires a second input that functions similar to rapamycin but does not interfere with the FKBP-FRB dimerization process. To this end, we used a second CID system that is functionally orthogonal to its rapamycin-based counterpart: GID (gibberellin insensitive dwarf 1) and GAIs (gibberellin insensitive shortened) dimerization as mediated by a synthetic gibberellin analog, GA₃-AM.¹⁴ To grant both CID systems equivalent functionality in attenuation of the Tiam1 fluorescence signal at the PM, we fused a single protein module of each CID system to the PM-localized Tiam1 protein (Supporting Information Figure 2a). This amounted to the design of the GAIs-YFP-Tiam1-FKBP-C2(LACT) construct which we coexpressed with the corresponding CID binding protein pairs placed in the Tom20-mCherry-GID and Tom20-CFP-FRB mitochondrial proteins in COS-7 cells (Figure 2b). We first confirmed the expected localization of each construct (Supporting Information Figure 2b). Addition of 100 nM rapamycin, 10 μM GA₃-AM, or a combination of both inputs successfully initiated the movement of the Tiam1-containing construct away from the PM toward the mitochondria, a function not rendered with the null DMSO input (Figure 2c and Supporting Information Figure 2b). Thus, the Tiam1 PM fluorescence reported by the GAIs-YFP-Tiam1-FKBP-C2(LACT) remained *high* only for the null DMSO input as expected for the NOR logic (Supporting Information Figure 2c). The attenuation of the PM localized fluorescence signal determined for the rapamycin input case was statistically significant ($p = 1.9 \times 10^{-3}$) 1 min post-input addition, indicating minute time scale execution of NOR logic (Supporting Information Figure 2d).

We then devised the NAND logic by continuing to employ the two orthogonal CID systems. For the NAND operation, Tiam1 had to be initially restricted to the PM, and only upon the presence of both rapamycin and GA₃-AM inputs could the Tiam1 be mobilized away from the PM (Figure 2d). This constraint suggested a two-step process: rapamycin attaching an actuation module to PM-localize Tiam1, and GA₃-AM using

this module to deliver Tiam1 to the mitochondria (Supporting Information Figure 3a). To implement this configuration, we expressed YFP-Tiam1-FKBP-C2(LACT), FRB-mCherry-GAIs, and Tom20-CFP-GID protein constructs in COS-7 cells (Figure 2e), each of which localized to the expected intracellular compartments (Supporting Information Figure 3b). FRB-mCherry-GAIs moved toward mitochondria in response to the input conditions containing GA₃-AM (Supporting Information Figures 3b and c), thus keeping the PM-bound Tiam1 unperturbed. Rapamycin, on the other hand, translocated the FRB-mCherry-GAIs to the PM, leaving the Tiam1 localization intact. Yet, GA₃-AM and rapamycin together, facilitated the translocation of YFP-Tiam1-FKBP-C2(LACT) away from the PM to the mitochondria. Consequently, the Tiam1 fluorescence signal at the PM was turned off exclusively in the presence of both inputs (Figure 2f), indicating successful implementation of the NAND logic expression (Supporting Information Figure 3d). Furthermore, similar to the NOT and NOR gates the device activation onset was determined to be within 1 min post-input addition (Supporting Information Figure 3e).

We next aimed to extend our technique to accommodate a negating Boolean logic operator which required the *low* rather than the *high* output to be initially present: the N-IMPLY function. Contrary to the NAND and NOR gates, the Tiam1 molecules had to be initially absent from the PM. Therefore, we placed Tiam1 in the cytoplasmic compartment. As the truth table suggests (Figure 2g), rapamycin had to take Tiam1 to the PM, whereas GA₃-AM had to direct it toward the mitochondria. For the double-input case, GA₃-AM had to offset the effect of rapamycin. This constraint suggested a competitive functionality of the two CID systems where the direction of Tiam1 motion was favored toward the GA₃-AM-mediated relocalization pathway (Supporting Information Figure 4a). Consequently, we used the GAIs-YFP-FKBP-C2(LACT), CFP-FRB-Tiam1, and Tom20-mCh-GID for expression in COS-7 cells (Figure 2h and Supporting Information Figure 4b). To bias the system toward the gibberellin-mediated translocation pathway,

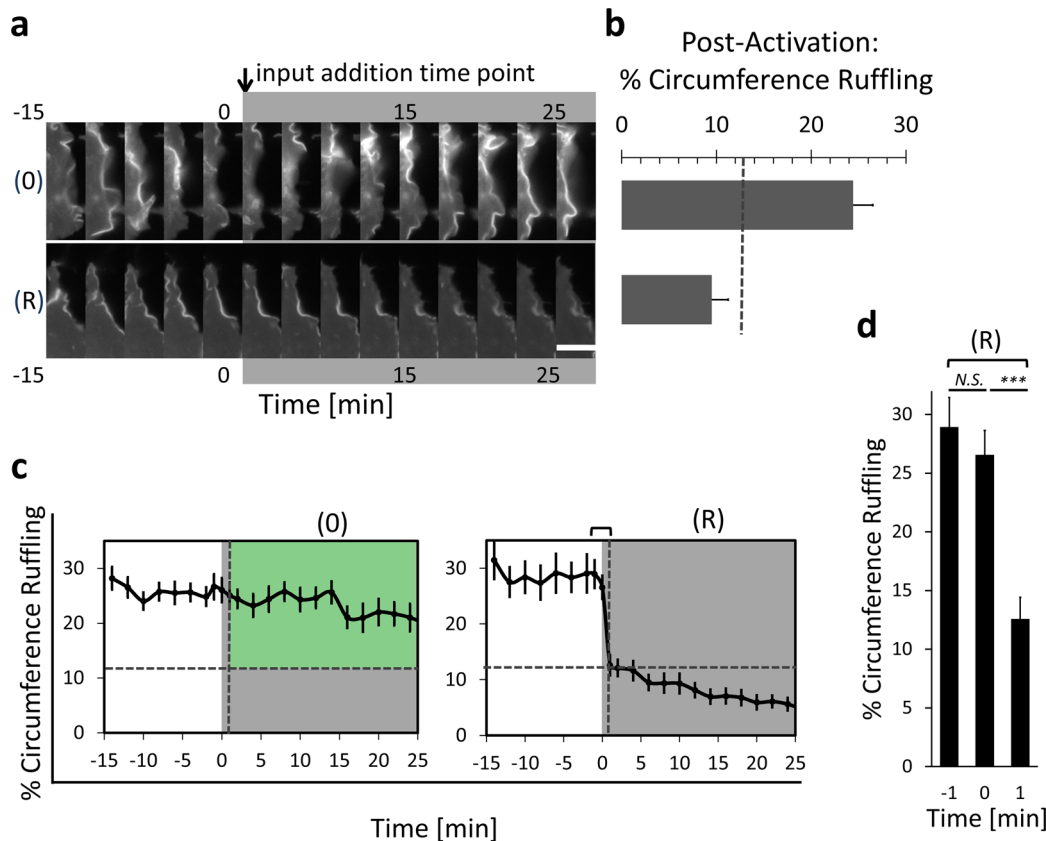


Figure 4. NOT gate. (a) Kymograph illustrating the ruffling extent of ~15% of a representative cell's circumference. The white scale bar is $10 \mu\text{m}$. The time interval in between each two consecutive frames is 3 min. The white PM curvatures correspond to the PM ruffling activity visualized by mCherry-CAAX PM marker. (b) The average PM ruffling activity reported at the fourth minute post-input addition. The dashed vertical line marks 12.6% device activation cutoff. (c) PM ruffling activity over the course of 40 min. Average values of ruffling activity are denoted as the percentage of the circumference ruffling. Zero on the horizontal axis marks the input addition time point. The gray shaded region illustrates the time interval when input was present. The dashed vertical line crosses the time axis at the device activation onset. The dashed horizontal line is at 12.6% marking the cutoff defining the device *high* or *low* output. The shaded green region defines the device *high* output. (0) and (R) stand for DMSO and rapamycin, respectively. (d) Student *t* test determining the device activation time. Assessment of significance of ruffling activity change 1 min pre- and post-input addition (marked with brackets on panel c). NS is $p = 0.04$, and *** denotes $p = 6.7 \times 10^{-6}$. This analysis was done for the rapamycin input case. All average values are reported using $n = 12$ cells from three independent experiments. All the error bars represent the standard error of the mean (SEM).

we used a higher concentration of GA₃-AM (100 μM) as compared to the NAND and NOR devices, while keeping the rapamycin concentration the same (100 nM). The CFP-FRB-Tiam1 translocation from the cytoplasm toward the PM occurred optimally only when rapamycin was present (Figure 2i and Supporting Information Figure 4b and c). The cytosolic CFP-FRB-Tiam1 signal was also depressed for the dual input case as GA₃-AM mediated the entrapment of Tiam1 at the mitochondria. Thus, the high PM Tiam1 fluorescence signal was observed exclusively for the rapamycin-only input case, indicating execution of N-IMPLY logic (Supporting Information Figure 4d). Tiam1 started moving away from the cytosolic region within 1 min after rapamycin was added (Supporting Information Figure 4c); however, the change in fluorescence intensity of Tiam1 at the PM was statistically significant ($p = 8.6 \times 10^{-3}$) 10 min post-rapamycin addition (Supporting Information Figure 4e), indicating a slower device activation time relative to the NOT, NOR, and NAND gates devised. However, this apparent lag was caused by the different quantification applied here; the fluorescence change was quantified at the PM instead of the cytosol.

After successful implementation of the NOT, NAND, NOR, and N-IMPLY logic expressions we looked into a physiological output likely generated through networking of the Tiam1 synthetic logic devices to an endogenous Rac signaling circuit (Figure 3). Tiam1 localization at the PM should activate Rac and its downstream signaling circuits that lead to formation of ruffling and lamellipodia.²² These membrane structures play a crucial role in cell motility and phagocytosis.²³ The CAAX PM marker is an apt choice for tracking and quantifying the ruffling extent²⁴ since in case of ruffling more membrane accumulates at the cell boundary and consequently the CAAX fluorescent signal increases. Thus, using this CAAX membrane marker transfected in cells, we visualized the membrane ruffles in the cell populations that contained our negating logic devices. For the NOT gate upon addition of the null DMSO input we observed no change in the extent of membrane ruffles, whereas the ruffling activity subsided with the rapamycin input (Figure 4a). This implied that the endogenous Rac circuitry in the cells executed a YES function, yielding the *high* ruffling output only when Tiam1 was present at the PM. We furthermore quantified the ruffling extent by analyzing the cells that met the criteria for expression level of each protein module (Methods). The

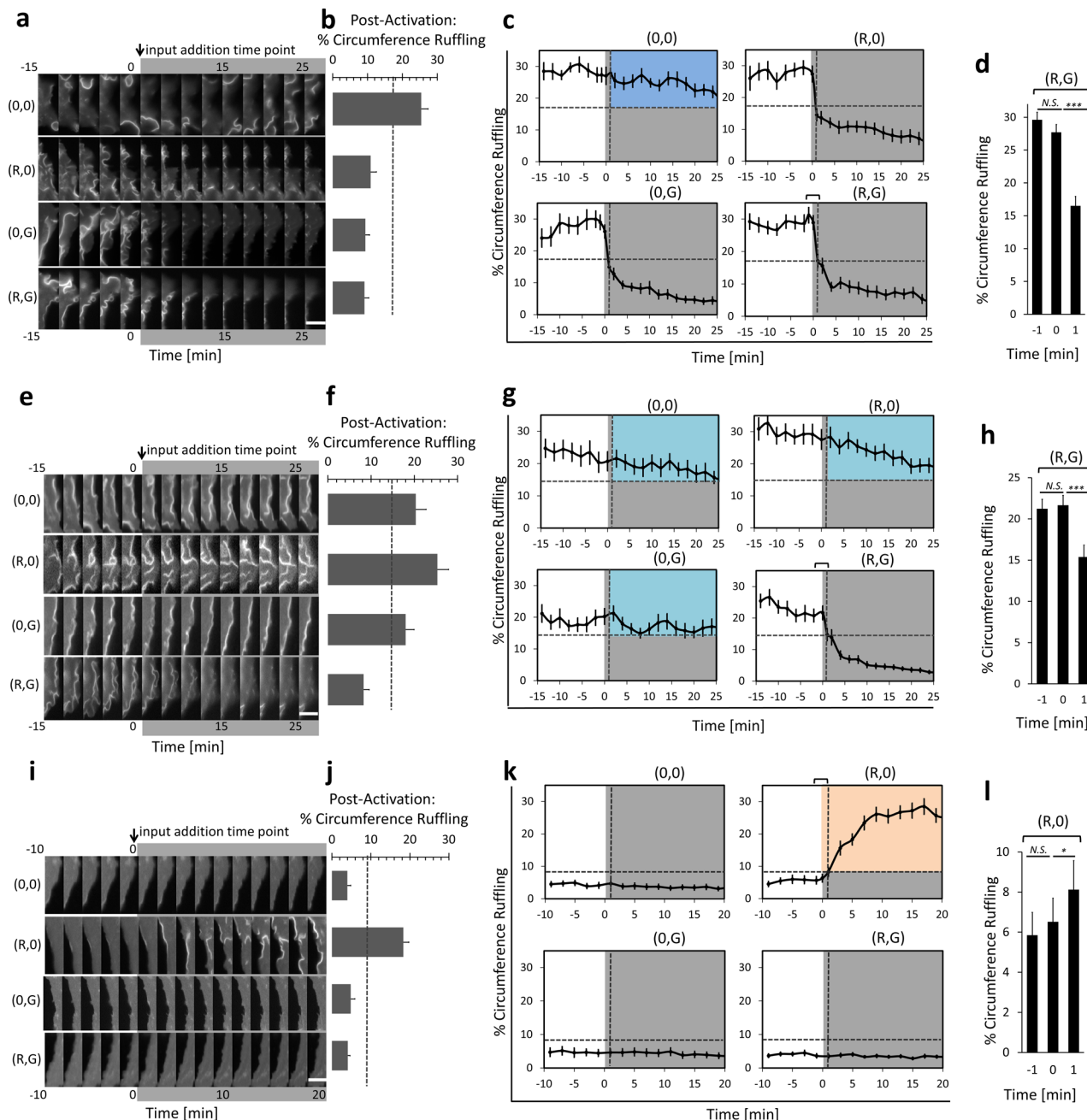


Figure 5. INOR device. (a) Kymograph illustrating the evolution of the ruffling activity of ~15% circumference of a representative cell over the course of 40 min. Three minutes lapse between two consecutive frames. (b) Average value of ruffling extent at the fourth minute post-input addition. The device activation onset evaluated as 17.1%, marked by the dashed line. (c) Dynamics of ruffling activity over the course of 40 min. The dashed horizontal line depicts the cutoff (17.1%) evaluated based on the ruffling extent of (R,G) case, 1 min post-input addition. (d) Determination of the NOR device activation onset considering the (R,G) condition. (NS is $p = 0.011$ and *** is $p = 3.4 \times 10^{-5}$). NAND device. (e) Same as panel a. (f) Average value of ruffling extent at the fourth minute post-input addition. The device activation threshold at 14.7%. (g) Dynamics of ruffling activity over the course of 40 min. The 14.7% activation cutoff was determined based on the extent of ruffling activity of (R,G) case, 1 min post-input addition. (h) Determination of the NAND device activation onset considering the (R,G) condition (NS is $p = 0.3$ and *** is $p = 1.3 \times 10^{-4}$). N-MPLY device. (i) Kymograph illustrating the evolution of the ruffling activity of ~15% circumference of a representative cell over the course of 30 min. Time elapsed between two consecutive frames is 2 min. (j) Average value of ruffling extent at 5 min post-input addition. The dashed vertical line represents the device activation threshold evaluated as 8.8%. (k) Dynamics of ruffling activity over the course of 30 min. The 8.8% activation threshold determined based on the extent of ruffling activity of (R,0) case, 1 min post-input addition. (l) Determination of N-MPLY device activation onset at 1 min post-input addition considering the (R,0) condition. (NS is $p = 0.09$ and * is $p = 0.7 \times 10^{-2}$). Binary inputs are denoted as follows: (0,0) for DMSO, (R,0) for rapamycin, (0,G) for GA₃-AM, (R,G) for rapamycin and GA₃-AM. The white scale bar represents 10 μ m. Average values presented are calculated considering more than 12 cells from three independent experiments. All the error bars represent SEM. Due to the decaying nature of the ruffling activity over time, $p < 0.01$ was considered statistically significant. The gray shaded region illustrates the time interval within which input was present. The dashed vertical line represents the device *high* versus *low* output.

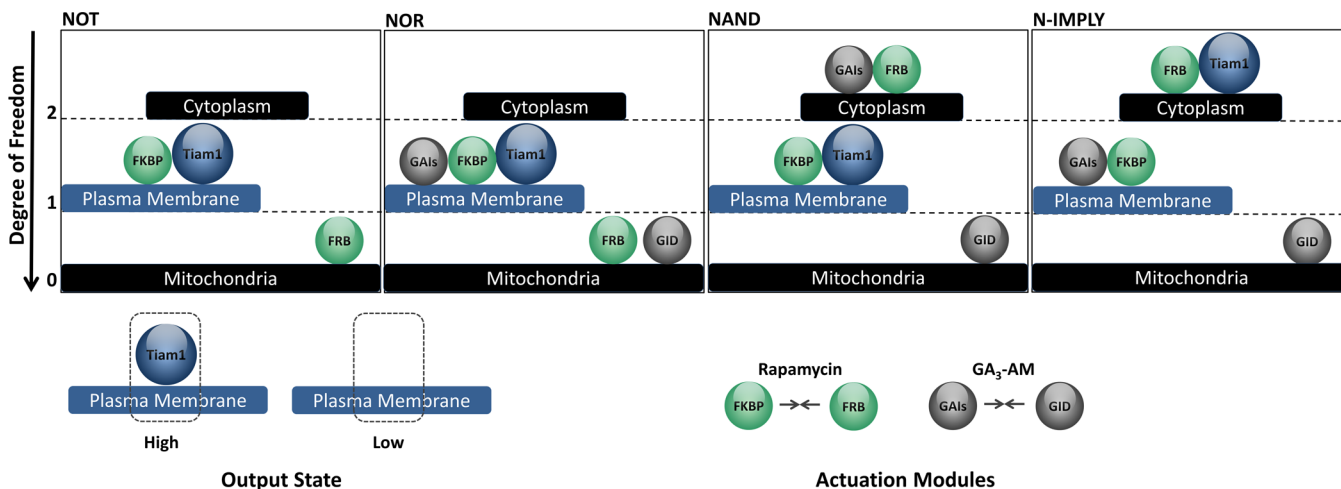


Figure 6. |Schematic of the discrete landscape representing the three levels of freedom in movement of protein modules which govern the output of each negating logic device. All the devices are depicted at the initial time-point, representing the (0,0) input case. Rapamycin facilitates binding of FKBP- and FRB-fusion proteins whereas GA₃-AM mediates pairing of GAI- and GID-containing protein constructs. The direction of these translocation movements are toward the compartment with the lower degree of freedom. Tiam1 presence on the plasma membrane contributes to the *high* output readout. The spheres placed adjacent to each other represent a fusion construct that translocates as a whole. Mitochondria is the location of maximum stability which hosts the molecules that are no longer free to move.

average values of PM ruffles 4 min after addition of DMSO or rapamycin were observed to be $24.4 \pm 2.3\%$ and $9.5 \pm 1.4\%$ of the total PM length, respectively (Figure 4b). The magnitude of these values with respect to the calculated activation threshold ($12.6 \pm 1.8\%$) indicated the robustness of the synthetic NOT logic gate and its efficacy in activating the endogenous Rac (Figure 4c). At basal level, on average, 30% of cells' circumference ruffled. The synthetic NOT function drove down this ruffling activity to 5% by the end of the experiment only for the *high* input case (Figure 4c and Supporting Information Movie 1). We assessed the change in ruffling activity to be statistically significant ($p = 6.7 \times 10^{-6}$) (Figure 4d) at 1 min post-input addition, and thus, we deemed the device active at this time point.

Following the same methodology, we evaluated the ruffling activity of the binary input gates. Cells containing the synthetic NOR gates ruffled only for the null input case as expected for NOR expression (Figure 5a and Supporting Information Movie 2). The average ruffling extent for each combination of inputs relative to the activation cutoff value set for the NOR device ($17.1 \pm 2.1\%$ cell circumference) was indicative of the robust operation of this logic device (Figure 5b). For all the input conditions except the null DMSO input, the PM ruffling extent diminished from an initial average value of 28% PM length to 5% by the end time point (Figure 5c). The output ruffling activity shows a sharp response with respect to small changes in Tiam1 concentration. For the (0,G) and (R,G) inputs, Tiam1 translocation away from the PM was not as efficient as the (0,R) case (Figure 2c), however it was sufficient to drive the ruffling output to saturation at a comparably low value, within a similar time scale (Figure 5c). The NOR device responded to the binary input within 1 min (Figure 5d). The synthetic NAND device also induced formation of ruffles following a NAND pattern (Figure 5e and Supporting Information Movie 3). The average ruffling activity per input condition with respect to the $14.7 \pm 1.9\%$ device activation cutoff indicated the successful operation of the NAND logic device cascaded to Rac as a YES operator (Figure 5f). The PM ruffling activity fell below the activation threshold, to a final value of 3%, only in

the presence of both inputs (Figure 5g). The NAND device activation time also remained within 1 min post-input addition (Figure 5h). Finally the synthetic N-IMPLY logic networked to the Rac pathway executed the N-IMPLY pattern of ruffle formation (Figure 5i and Supporting Information Movie 4). The average length of circumference ruffling was only above the activation threshold ($8.5 \pm 1.4\%$) for the rapamycin input case ($18.3 \pm 1.4\%$), indicating execution of N-IMPLY logic (Figure 5j). We assessed the onset of ruffling suppression to be within a minute (Figures 5k and 5l). In the cellular context presented, this N-IMPLY functionality allows for controlling signaling in a reversible manner given the two dimerizers are added sequentially instead of simultaneously.²⁴

In our study, the Rac signaling pathway as a whole served as a YES gate and enabled us to engage a synthetic device with an endogenous signaling circuit in order to execute a biologically relevant output. This prompted us to consider examining signal transduction pathways as biological circuits' analogues and screen for logic patterns in endogenous pathways. Specifically, we counted the number of OR, AND, NOR, NAND, IMPLY, and N-IMPLY logic topologies that do not emerge as a result of networking (Supporting Information Methods). Such minimal logic configurations were expected to assume the topology of a three-nodal motif where the two nodes representing the inputs either both promote the output node (OR/AND) (Supporting Information Figure 5a and b), both inhibit the output (NOR/NAND) (Supporting Information Figure 5c and d), or one promotes and the other inhibits the output (IMPLY/N-IMPLY) (Supporting Information Figure 5e and f). We surveyed the prevalence of these logic patterns in 108 well-annotated signaling pathways (Supporting Information Data File 1). We found 775 OR/AND, 26 NOR/NAND, and 198 IMPLY/N-IMPLY logic patterns. Given the total inhibition and forward reactions available to cells, the calculated expected value for each of these logic topologies were 765, 16, and 219, respectively (Supporting Information Data Files 2 and 3).

NOR and NAND logic gate patterns are the most efficacious in the electronics context as either of these gates alone can be used to implement any other logic operations, a property

known as *universality*. This overutilization of a single logic element in electronics does not seem to be a feature used in cell signaling. We further screened for the number of NOR/NAND patterns cascaded to each other (Supporting Information Figure 6). Despite the 26 NOR/NAND hits likely being an overestimation of the number of actual NOR/NAND gates, we did not find any instance of *universal* gates cascading (0 out of 405 logic gate cascades) (Supporting Information Data File 2). This further suggests that native cell signaling pathways do not resort to universal logic functions to navigate their finite resources. Endogenous inhibitory molecules appear in a hub, and disseminate their signals downstream through suppression of several activator molecules rather than directly networking. Perhaps repeated use of inhibitory signal is more costly than a single use of signal activation. Arguably, not all the conventions in Boolean algebra, in their strict sense, apply in nature.

Further analysis and experiments are needed to verify that the three-nodal patterns identified indeed constitute the corresponding logic function. However, for cases like the regulation of microtubule associated protein 1B (MAP1B) by two protein phosphatases (PP1 and PP2A), the current literature confirms the existence of the NOR logic function.²⁵ Because of the limited number of CID systems at hand our synthetic device can only generate a single output for probing signaling pathways like Rac. Expanding our system to a binary output device would allow manipulating these signaling pathways with two inputs to further investigate the true logic identity of such endogenous networks.

In summary, we created logic devices with physiological outputs that functioned within a minute in live cells. These devices could also control the concentration of a gene product within various subcellular spaces. We accomplished this design by feeding the output of our synthetic NOT, NOR, NAND, and N-IMPLY logic devices into the Rac signaling pathway. These synthetic devices themselves executed negation by orchestrating Tiam1 movement within cells, without utilizing molecular suppressors usually used to implement the NOT function. Our design consisted of a three-state movement landscape, where each state represented a subcellular space, and imposed a distinct degree of freedom in movement on its resident molecules (Figure 6). By using CID systems we induced the movement of the activator molecule in between the spaces, in the direction of increasing constraint, and thus created negation. The engineered synthetic devices were used to probe signaling networks in order to create physiological outputs and understand the dynamics of cell signaling. In the future studying synthetic negating logic devices with identical inputs/outputs and varied pathway lengths will be of interest. Because of their fast speed, the networked pathways composed of cascaded post-translational *universal* logic gates will also prove useful in biomolecular computation. Moreover, generating an oscillatory output signal, or implementing the exclusive negating family of gates (XNOR) are avenues of research to be explored in the future. Given the higher specificity inherent in two-input logic gates to environmental variables, emulating the same negating functions wired to alternative input and output terminals is valuable for detection of biological molecules, and potentially medical diagnosis. Such diagnostic devices can take pathogenic substances or disease biomarkers as inputs, and yield a fast detect-to-protect response that is crucial for applications in biowarfare or early disease detection.

METHODS

DNA Constructs. Molecular cloning of mCherry-CAAX, Tom20-mCh-FRB, Tom20-CFP-FRB, Tom20-CFP-GID, Tom20-mCh-GID, and CFP-FRB-Tiam1 have been reported elsewhere.^{14,24,26} For construction of GAI_s-YFP-FKBP-C2(LACT), the PCR product encoding C2(LACT) using PCR primers (forward, GAGAATTCTATGCGCCAATCCCTGG-GGC; reverse, GCTGGATCCGTACAAGAAAGCTGG-GTTCTAACAG) was inserted into GAI_s-YFP-FKBP¹⁴ using the EcoRI and BamHI sites. For the construction of GAI_s-YFP-Tiam1-FKBP-C2(LACT), Tiam1 was digested out from GID-Tiam1-YFP-CAAX and inserted in GAI_s-YFP-FKBP-C2(LACT) using the BsrGI sites. For construction of YFP-Tiam1-FKBP-C2(LACT), the Tiam1 insert obtained from digestion of GAI_s-YFP-Tiam1-FKBP-C2(LACT) was ligated into YFP-FKBP-C2(LACT)²⁴ using the BsrGI sites. For construction of FRB-mCherry-GAI_s, GAI_s was digested out from CFP-GAI_s and inserted into FRB-mCherry using the EcoRI and BamHI sites.

Cell Culture and Transfection. COS-7 cells were cultured in DMEM (GIBCO) medium supplemented with 10% FBS and 1% Penicillin Streptomycin (Life Technologies) placed in a 5% CO₂ incubator. Cells were split every 2 days. For transfection, coverglass thinly coated with 1 mg/mL of poly-d-lysine (Sigma) placed in 6-well plates were used to plate COS-7 cells mixed with 5 μL Turbofect (Fermentas) and the transfection mixture. The transfection mixture contained 1 μL of 1 μg/μL of each DNA construct defined for each logic gate, mixed with 37.5 μL of Opti-MEM (Life Technologies).

Live Cell Imaging. The transfected cells were incubated (5% CO₂, 37 °C) for 24 h prior to imaging. Cells were imaged in DMEM containing 25 mM HEPES (GIBCO). Live cell imaging was performed using an inverted epi-fluorescence microscope (Axiovert135TV, ZEISS) using a 40× oil objective. Fluorescence images were collected by a QIClick charge-coupled device camera (QImaging). Exposure time per fluorescence channel was 200 ms, and the images were obtained at a frequency of 1 frame per minute for 30 to 40 min experiment duration, depending on the logic device. Rapamycin was obtained from LClab and GA₃-AM was prepared as described previously.¹⁴ Rapamycin and GA₃-AM both were dissolved in DMSO. The zero input case consisted of DMSO alone. All of these inputs were resuspended in DMEM containing HEPES media before they were added to the sample chamber.

Image Analysis, Fluorescence Intensity Measurement, and Ruffling Quantification. The localization of each protein construct was verified. The intensity of the fluorescent protein signal in the localization region of interest relative to the background was measured using Metamorph software (Molecular Devices). To account for photobleaching the decay in fluorescence signal 10 min prior to input addition was measured and the data were corrected considering a linear photo bleaching trend. The fluorescence signal at each time point was normalized by the average value of fluorescence signal 10 min before the inputs were added.

For the ruffling analysis, the range of ratios within which each device executed the logic robustly was measured (the performance was assessed by quantification of the ruffling activity as described below). On the basis of this, the rubric for acceptable fluorescence intensity ranges was determined. For all the experiments only cells which expressed protein within this

ratiometric intensity were analyzed. To quantify the PM ruffles the Trace Region feature in the toolbar of Metamorph software was used to measure the circumference of each cell at the initial time point (denoted as L). The length of PM ruffles for every other time point was measured (denoted as R_i where i indicates the time point). The R_i/L ratio was used to report the circumference of cell ruffling for any given time point.

Statistical Analysis. Paired, single-tailed, Student's *t*-test (Microsoft Excel) determining the statistical significance of ruffling activity change 1 min prior to input addition and 1 min post-input addition was performed. For the NOT gate, this was done for the rapamycin input condition. For the NOR gate, this analysis was done for the (rapamycin, GA₃-AM) input condition as the drop in ruffling activity post-input treatment was the least drastic for this case, marking the worst-case scenario. For the NAND gate, this analysis was done on the (rapamycin, GA₃-AM) condition since only for this case we expected and observed a change in ruffling activity. For the N-IMPLY device, this analysis was done for the (rapamycin, 0) condition as only for this case a change in ruffling activity was expected and observed. Because of the high exposure time, background decay in ruffling activity was observed over the course of the experiment. We mainly defined $p < 0.01$ as statistically significant.

■ ASSOCIATED CONTENT

Supporting Information

Supplemental methods, additional figures, and the accompanying texts, movie files, and tabulated data files. This material is available free of charge *via* the Internet at <http://pubs.acs.org>.

■ AUTHOR INFORMATION

Corresponding Author

*E-mail: jctinoue@jhmi.edu.

Author Contributions

S.R. and T.I. conceived the experimental design. S.R. and T.I. generated the DNA constructs. S.R. carried out the cell biology experiments and analyzed the experimental data. S.S. performed the computational screening. S.R. and T.I. wrote the manuscript.

Notes

The authors declare no competing financial interest.

■ ACKNOWLEDGMENTS

We are grateful to T. Miyamoto, Y. Lin, and Y. Nihongaki for assistance and insightful suggestions on the experiments. We also thank M. Ostermeier, D. Yue, R. DeRose, B. Lin, P. Razavi, and J. Senarathna for critical comments on the manuscript. This work was supported by Japan Science and Technology Agency (10216 to T.I.) and the National Institute of Health (GM092930 to T.I.). S.R. is supported by the National Institute of Health Training Program in Translational Research in Imaging (T32 EB010021 to Dr. Elliot McVeigh).

■ REFERENCES

- (1) Benenson, Y. (2012) Biomolecular computing systems: Principles, progress and potential. *Nat. Rev. Genet.* 13, 455–68.
- (2) Macia, J., and Sole, R. (2014) How to make a synthetic multicellular computer. *PLoS One* 9, e81248.
- (3) Miyamoto, T., Razavi, S., DeRose, R., and Inoue, T. (2013) Synthesizing biomolecule-based Boolean logic gates. *ACS Synth. Biol.* 2, 72–82.
- (4) Lakin, M. R., Youssef, S., Cardelli, L., and Phillips, A. (2012) Abstractions for DNA circuit design. *J. R. Soc. Interface* 9, 470–86.
- (5) Goñi-Moreno, A., and Amos, M. (2012) A reconfigurable NAND/NOR genetic logic gate. *BMC Syst. Biol.* 6, 126.
- (6) Hemphill, J., and Deiters, A. (2013) DNA computation in mammalian cells: microRNA logic operations. *J. Am. Chem. Soc.* 135, 10512–8.
- (7) Gaber, R., Lebar, T., Majerle, A., Šter, B., Dobnikar, A., Benčina, M., and Jerala, R. (2014) Designable DNA-binding domains enable construction of logic circuits in mammalian cells. *Nat. Chem. Biol.* 10, 203–8.
- (8) Wang, B., Kitney, R. I., Joly, N., and Buck, M. (2011) Engineering modular and orthogonal genetic logic gates for robust digital-like synthetic biology. *Nat. Commun.* 2, 508.
- (9) Bonnet, J., Yin, P., Ortiz, M. E., Subsoontorn, P., and Endy, D. (2013) Amplifying genetic logic gates. *Science* 340, 599–603.
- (10) Samiappan, M., Dadon, Z., and Ashkenasy, G. (2011) Replication NAND gate with light as input and output. *Chem. Commun. (Camb)* 47, 710–2.
- (11) Zhou, N., Windmiller, J. R., Valdés-Ramírez, G., Zhou, M., Halámková, J., Katz, E., and Wang, J. (2011) Enzyme-based NAND gate for rapid electrochemical screening of traumatic brain injury in serum. *Anal. Chim. Acta* 703, 94–100.
- (12) Zhou, J., Arugula, M. A., Halámková, J., Pita, M., and Katz, E. (2009) Enzyme-based NAND and NOR logic gates with modular design. *J. Phys. Chem. B* 113, 16065–70.
- (13) Privman, V., Pedrosa, V., Melnikov, D., Pita, M., Simonian, A., and Katz, E. (2009) Enzymatic AND-gate based on electrode-immobilized glucose-6-phosphate dehydrogenase: towards digital biosensors and biochemical logic systems with low noise. *Biosens. Bioelectron.* 25, 695–701.
- (14) Miyamoto, T., DeRose, R., Suarez, A., Ueno, T., Chen, M., Sun, T. P., Wolfgang, M. J., Mukherjee, C., Meyers, D. J., and Inoue, T. (2012) Rapid and orthogonal logic gating with a gibberellin-induced dimerization system. *Nat. Chem. Biol.* 8, 465–70.
- (15) Lambert, J. M., Lambert, Q. T., Reuther, G. W., Malliri, A., Siderovski, D. P., Sondek, J., Collard, J. G., and Der, C. J. (2002) Tiam1 mediates Ras activation of Rac by a PI(3)K-independent mechanism. *Nat. Cell Biol.* 4, 621–5.
- (16) DeRose, R., Miyamoto, T., and Inoue, T. (2013) Manipulating signaling at will: Chemically-inducible dimerization (CID) techniques resolve problems in cell biology. *Pflügers Arch.* 465, 409–17.
- (17) Fegan, A., White, B., Carlson, J. C., and Wagner, C. R. (2010) Chemically controlled protein assembly: Techniques and applications. *Chem. Rev.* 110, 3315–36.
- (18) Spencer, D. M., Wandless, T. J., Schreiber, S. L., and Crabtree, G. R. (1993) Controlling signal transduction with synthetic ligands. *Science* 262, 1019–24.
- (19) Yeung, T., Gilbert, G. E., Shi, J., Silvius, J., Kapus, A., and Grinstein, S. (2008) Membrane phosphatidylserine regulates surface charge and protein localization. *Science* 319, 210–3.
- (20) Neuspil, M., Schauss, A. C., Braschi, E., Zumino, R., Rippstein, P., Rachubinski, R. A., Andrade-Navarro, M. A., and McBride, H. M. (2008) Cargo-selected transport from the mitochondria to peroxisomes is mediated by vesicular carriers. *Curr. Biol.* 18, 102–8.
- (21) Gao, J., Liao, J., and Yang, G. Y. (2009) CAAX-box protein, prenylation process and carcinogenesis. *Am. J. Transl. Res.* 1, 312–25.
- (22) Heasman, S. J., and Ridley, A. J. (2008) Mammalian Rho GTPases: new insights into their functions from *in vivo* studies. *Nat. Rev. Mol. Cell Biol.* 9, 690–701.
- (23) Minard, M. E., Kim, L. S., Price, J. E., and Gallick, G. E. (2004) The role of the guanine nucleotide exchange factor Tiam1 in cellular migration, invasion, adhesion and tumor progression. *Breast Cancer Res. Treat.* 84, 21–32.
- (24) Lin, Y. C., Nihongaki, Y., Liu, T. Y., Razavi, S., Sato, M., and Inoue, T. (2013) Rapidly reversible manipulation of molecular activity with dual chemical dimerizers. *Angew. Chem., Int. Ed.* 52, 6450–4.
- (25) Sontag, J. M., Nunbhakdi-Craig, V., White, C. L., Halpain, S., and Sontag, E. (2012) The protein phosphatase PP2A/B α binds to the

microtubule-associated proteins Tau and MAP2 at a motif also recognized by the kinase Fyn: Implications for tauopathies. *J. Biol. Chem.* 287, 14984–93.

(26) Komatsu, T., Kukelyansky, I., McCaffery, J. M., Ueno, T., Varela, L. C., and Inoue, T. (2010) Organelle-specific, rapid induction of molecular activities and membrane tethering. *Nat. Methods* 7, 206–8.